Inorg. Chem. **2002**, *41*, 3491–3499

Five-Coordinate Complexes $[FeX(depe)_2]BPh_4$, X = Cl, Br: Electronic Structure and Spin-Forbidden Reaction with N_2†

Oliver Franke,‡ Beatrix E. Wiesler,§ Nicolai Lehnert,‡ Christian Näther,‡ Vadim Ksenofontov,§ Jörg Neuhausen,|| and Felix Tuczek*,‡

Christian Albrechts Universität Kiel, Otto Hahn Platz 6/7, D-24098 Kiel, Germany, Johannes Gutenberg Universität Mainz, Staudingerweg 9, D-55099 Mainz, Germany, and Johannes Gutenberg Universität Mainz, Becherweg 25, D-55099 Mainz, Germany

Received November 26, 2001

The bonding of N_2 to the five-coordinate complexes $[FeX(depe)_2]^+$, X = Cl (**1a**) and Br (**1b**), has been investigated with the help of X-ray crystallography, spectroscopy, and quantum-chemical calculations. Complexes **1a** and **1b** are found to have an XP_4 coordination that is intermediate between square-pyramidal and trigonal-bipyramidal. Mössbauer and optical absorption spectroscopy coupled with angular overlap model (AOM) calculations reveal that **1a** and **1b** have $^3B_1$ ground states deriving from a $(xz)^1(z^2)^1$ configuration. The zero-field splitting for this state is found to be 30–35 cm^{-1}. In contrast, the analogous dinitrogen complexes $[FeX(N_2)(depe)_2]^+$, X = Cl (**2a**) and Br (**2b**), characterized earlier are low-spin ($S = 0$; Wiesler, B. E.; Lehnert, N.; Tuczek, F.; Neuhausen, J.; Tremel, W. *Angew. Chem, Int. Ed.* **1998**, *37*, 815–817). N_2 bonding and release in these systems are thus spin-forbidden. It is shown by density functional theory (DFT) calculations of the chloro complex that the crossing from the singlet state (ground state of **2a**) to the triplet state (ground state of **1a**) along the Fe–N coordinate occurs at $r_C = 2.4$ Å. Importantly, this intersystem crossing lowers the enthalpy calculated for N_2 release by 10–18 kcal/mol. The free reaction enthalpy $\Delta G°$ for this process is calculated to be 4.7 kcal/mol, which explains the thermal instability of N_2 complex **2a** with respect to the loss of N_2. The differences in reactivity of analogous *trans* hydrido systems are discussed.

Introduction

Nitrogen fixation continues to present a fascinating and challenging problem to many scientific disciplines ranging from inorganic chemistry to molecular biology.[1,2] As a part of our ongoing efforts to investigate the conditions for the metal-centered reduction and protonation of dinitrogen,[3,4] we also became interested in the process of N_2 binding which represents the initial step along this reaction pathway. Because of the generally low affinity of Fe(II) toward N_2,[5] iron dinitrogen systems are ideal candidates to study this problem, particularly with respect to the requirements concerning the structure and geometry of the N_2 binding fragment, the influence of the coligands, and the electronic structure of the central atom. Moreover, iron plays a major role in the industrial as well as biological processes of nitrogen fixation[2,6] and, like other d^6 metal centers, is of interest as a potential candidate for the reproduction of the enzymatic reaction in vitro.[7,8]

In an earlier communication, we reported on the synthesis as well as the structural and spectroscopic characterization

* To whom correspondence should be addressed. E-mail: ftuczek@ac.uni-kiel.de.

† Dedicated to Prof. Dr. Dieter Sellmann on the occasion of his 60th birthday.

‡ Christian Albrechts Universität Kiel.

§ Johannes Gutenberg Universität Mainz, Staudingerweg 9.

|| Johannes Gutenberg Universität Mainz, Becherweg 25.

(1) Fryzuk, M.; Johnson, S. A. *Coord. Chem. Rev.* **2000**, *200*, 379−419.
(2) *Prokaryotic Nitrogen Fixation: A Model System for the Analysis of a Biological Process*; Triplett, E. W., Ed.; Horizon Scientific Press: Wymondham, U.K., 2000.
(3) (a) Lehnert, N.; Wiesler, E. B.; Tuczek, F.; Hennige, A.; Sellmann, D. *J. Am. Chem. Soc.* **1997**, *119*, 8869−8888. (b) Lehnert, N.; Tuczek, F. *Inorg. Chem.* **1999**, *38*, 1659−1682.
(4) Wiesler, E. B.; Lehnert, N.; Tuczek, F.; Neuhausen, J.; Tremel, W. *Angew. Chem., Int. Ed.* **1998**, *37*, 815−817.
(5) Tuczek, F.; Lehnert, N. *Angew. Chem., Int. Ed.* **1998**, *37*, 2636−2638.
(6) (a) *Catalytic Ammonia Synthesis: Fundamentals and Practice (Fundamental and Applied Catalysis)*; Jennings, J. R., Ed.; Plenum Publishing: New York, 1991. (b) Appl, M. *Ammonia: Principles and Industrial Practice*; Wiley-VCH: New York, 1999.
(7) (a) Hidai, M.; Mizobe, Y. *Chem. Rev.* **1995**, *95*, 1115−1133. (b) Henderson, R. A.; Leigh, G. J.; Pickett, C. *Adv. Inorg. Chem. Radiochem.* **1983**, *27*, 197−292.
(8) Sellmann, D.; Utz, J.; Blum, N.; Heinemann, F. W. *Coord. Chem. Rev.* **1999**, *190−192(0)*, 607−627.

10.1021/ic0111987 CCC: $22.00
Published on Web 06/05/2002

of the octahedral dinitrogen complex $[FeCl(N_2)(depe)_2]BPh_4$ (**2a**; depe = 1,2-bis(diethylphosphino)ethane).[4] Using Mössbauer spectroscopy, we found that this compound has an Fe−N_2 bond that is thermally labile at 300 K. Because **2a** itself exhibits a quadrupole doublet with $\delta_{IS} = 0.26$ and $\Delta E_Q = 1.40$ mm/s at 100 K, we attributed a second doublet with a much larger quadrupole splitting present in the Mössbauer spectra of **2a** to the corresponding dinitrogen-free species generated by thermal decay of **2a**. In addition, complex **2a** was found to be photosensitive releasing N_2 under UV−vis irradiation. Now we have directly isolated the compound $[FeCl(depe)_2]BPh_4$ (**1a**) from a methanolic solution of $[FeCl_2(depe)_2]$. Its Mössbauer parameters are almost identical with those of the dinitrogen-free species in the matrix of **2a** and thus support our earlier assignment. In a similar manner, we have also prepared the corresponding bromo complex $[FeBr(depe)_2]BPh_4$ (**1b**). This is related to the dinitrogen complex $[FeBr(N_2)(depe)_2]BPh_4$ (**2b**) which also exhibits the tendency to lose dinitrogen at room temperature.[4] In contrast, analogous hydride containing dinitrogen complexes $[FeH(N_2)(diphos)_2]^+$ (diphos = depe,[9a,b] dppe,[9c] and dmpe[9d]) appear to be thermally stable.[10a] Moreover, these systems and their five-coordinate precursors exhibit a remarkable stability toward O_2. Thus, $[FeH(dppe)_2]^+$ in a THF solution or in the solid-state picks up N_2 from air, leading to $[FeH(N_2)(dppe)_2]^+$.[10a,b] A methanolic solution of $[FeCl(depe)_2]^+$, on the other hand, is extremely air sensitive.[10a,11] To understand these drastic differences in reactivity between otherwise identical hydrido and halogeno complexes, we investigated in detail the geometric and electronic structures of the five-coordinate fragments $[FeX(depe)_2]^+$, X = Cl (**1a**) and Br (**1b**), by X-ray crystallography and spectroscopy (UV−vis absorption, Mössbauer). The optical absorption spectra are evaluated with the angular overlap model (AOM) leading to an unambiguous assignment of the electronic ground state. The bonding of N_2 in these systems is studied by density functional theory (DFT) calculations. A forthcoming paper will describe analogous investigations on the corresponding five-coordinate hydrido systems and their six-coordinate dinitrogen adducts.[12]

Experimental Section

Synthetic Procedures and Physical Methods. Synthesis and handling of all compounds were performed in inert gas atmosphere by use of Schlenk techniques and gloveboxes. All solvents were dried following literature procedures. Reagents and the phosphine ligand 1,2-bis(diethylphosphino)ethane (depe) were obtained from commercial sources and used without further purification. UV−vis spectra were measured with a Varian CARY 5 UV−vis−NIR spectrometer. Mössbauer spectra were recorded with a WISSEL setup equipped with a He flow-through cryostat (Oxford CF506); isomer shifts are quoted versus α-Fe. Magnetic susceptibility was measured with a Physical Instruments (PI) vibrating sample (Foner) magnetometer. Susceptibility data were corrected for diamagnetic contributions using Pascal's constants.

Crystal Structure Determinations. Intensity data of compound **1a** were collected using a Siemens P4 four-circle diffractometer,[13] and those of compound **1b**, using a STOE imaging plate diffraction system using Mo Kα radiation. All structures were solved with direct methods using SHELXS-86 for compound **1a** and SHELXS-97 for compound **1b**. Refinement was done against F^2 using SHELXL-93. In **1a**, all non-H atoms were refined anisotropically. In the subsequent refinement, the H atoms were positioned with idealized geometry and isotropic temperature parameters. In one of the crystallographically independent complex cations of compound **1b**, one phosphorus atom and five carbon atoms are disordered and were refined using a split model. All non-hydrogen atoms except P5, C2′, C21′, C22′, C23′, and C24′ in compound **1b** were refined using anisotropic displacement parameters. The hydrogen atoms were positioned with idealized geometry and refined using a riding model. Further information is contained in Tables 1 and 2 and in the Supporting Information.

Synthesis of $[FeX_2(depe)_2]$ (X = Cl, Br) (3a, 3b). These complexes were prepared following modified literature procedures.[14] A solution of depe (6 mmol) in 10 mL of toluene was added to a suspension of the appropriate anhydrous ferrous salt (3 mmol) in 30 mL of toluene. The reaction mixture was refluxed for 1 h resulting in a green (X = Cl) and yellow-green (X = Br) solution, respectively. After cooling to room temperature, the solution was filtered, and the volume of the filtrate was reduced to 20 mL. Cooling the filtrate to −40 °C for 2 days yielded a crystalline product which was separated by filtration and dried under vacuum. Purity was checked by elemental analysis.

Synthesis of $[FeX(depe)_2]BPh_4$ (X = Cl, Br) (1a, 1b). A mixture of $[FeX_2(depe)_2]$ (0.5 mmol) in 50 mL of methanol was allowed to stir overnight at room temperature under 1 atm of Ar, resulting in an orange solution. Addition of a solution of $NaBPh_4$ (1.1 mmol) in 10 mL of methanol slowly gave a crystalline product which was separated by filtration and dried under vacuum. Purity was checked by elemental analysis.

Synthesis of $[FeHCl(depe)_2]BPh_4$ (4). This complex was prepared following literature procedures.[15]

Crystallographic Characterization

The structure of **1a** consists of $[FeCl(depe)_2]^+$ cations and BPh_4^- anions (Table 1). The coordination geometry around the metal center is best described as square-pyramidal with a distortion toward trigonal-bipyramidal (Figure 1). A view of the first coordination sphere around the Fe ion (Figure 2) reveals that the chloro ligand is in apical position, perpendicular (within ±2°) to two of the four phosphorus atoms, P(2) and P(3), which form an almost linear P−Fe−P axis. The other two phosphorus atoms, P(1) and P(4), are bent

(9) (a) Bancroft, G. M.; Mays, J. J.; Prater, B. E. *J. Chem. Soc., Chem. Commun.* **1969**, 585. (b) Buys, I. E.; Field, L. D.; Hambley, T. W.; McQueen, A. E. D. *Acta Crystallogr.* **1993**, *C49*, 1056−1059. (c) Azizian, H.; Morris, R. H. *Inorg. Chem.* **1983**, *22*, 6−9. (d) Hills, A.; Hughes, D. L.; Jimenez-Tenorio, M.; Leigh, G. J. *J. Organomet. Chem.* **1990**, *391*, C41−C44.
(10) (a) Wiesler, B. E. PhD dissertation, University of Mainz, 1999. (b) Aresta, M.; Giannocaro, P.; Rossi, M.; Sacco, A. *Inorg. Chim. Acta* **1971**, *5*, 115−118.
(11) Bellerby, J. M.; Mays, M. J.; Sears, P. L. *J. Chem. Soc., Dalton Trans.* **1976**, 1232−1236.
(12) Franke, O.; Wiesler, B. E.; Tuczek, F. To be published.
(13) Details on this crystal structure determination have been deposited at Fachinformationszentrum Karlsruhe, D-76344 Eggenstein-Leopoldshafen, under the number CSD-410052.
(14) (a) Mays, M. J.; Prater, B. E. *Inorg. Synth.* **1974**, *15*, 21−29. (b) Evans, D. J.; Henderson, R. A.; Hills, A.; Hughes, D. L.; Oglieve, K. E. *J. Chem. Soc., Dalton Trans.* **1992**, 1259−1265.
(15) Wiesler, B. E.; Tuczek, F.; Näther, C.; Bensch, W. *Acta Crystallogr.* **1998**, *C54*, 44−46.

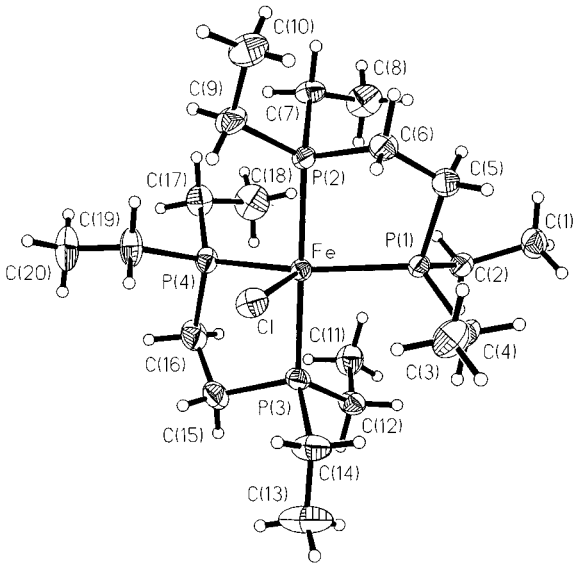

Figure 1. Perspective view of [FeCl(depe)$_2$]$^+$ (**1a**) (vibrational ellipsoids with 30% probability).

Table 1. Crystal and Refinement Data for Compounds **1a** and **1b**

	1a	**1b**
formula	$C_{44}H_{68}BClFeP_4$	$C_{44}H_{68}BBrFeP_4$
MW/g·mol^{-1}	822.97	867.43
cryst color	orange	orange
cryst syst	orthorhombic	triclinic
space group	$P2_12_12_1$	$P\bar{1}$
a, Å	10.935 (2)	13.209 (1)
b, Å	15.883 (1)	16.538 (1)
c, Å	25.520 (3)	23.213 (2)
α, °	90.00	107.46 (1)
β, °	90.00	96.05 (1)
γ, °	90.00	107.38 (1)
V, Å^3	4432.3 (1)	4509.4 (5)
temp, K	168	150
Z	4	4
D_{calcd}, g·cm^{-3}	1.233	1.278
F(000)	1760	1832
2θ range	4°−54°	3°−54°
$h/k/l$ ranges	−1/13, −1/20, −1/32	−16/16, −21/19, −29/29
abs corr	empirical	face-indexed
μ, mm^{-1}	0.574	1.39
max/min transm	0.836/0.735	0.761/0.841
measured reflns	6587	35419
R_{int}	0.0123	0.0372
independent reflns	6328	17838
reflns with $I > 2\sigma(I)$	5338	13801
refined params	455	943
R1 [$I > 2\sigma(I)$]	0.0309	0.0380
wR2 [all data]	0.0716	0.1027
GOF	0.940	1.049
min/max res, e·Å^{-3}	0.34/−0.24	0.92/−0.68
Flack x-parameter	0.008 (15)	

away from the Fe−Cl bond. In a trigonal bipyramid, the angles Cl−Fe−P(1), Cl−Fe−P(4), and P(1)−Fe-P(4) would be close to 120°, while the corresponding values in **1a** are 106°, 101°, and 152°, respectively. The resulting "open" face in this coordination sphere represents a potential site for attack of an additional ligand, for example, dinitrogen. Fe−Cl and Fe−P distances are within the range characteristic of related Fe(II) low-spin systems (2.18−2.36 Å); the P−Fe−P bite angle is about 84°, a typical value for the depe ligand.[9] Relevant bond distances and angles are listed in Table 2.

A comparison of **1a** with the related octahedral dinitrogen complex **2a** which has been characterized earlier[4] reveals

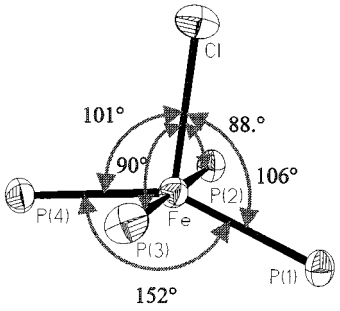

Figure 2. View of the first coordination sphere of **1a** showing the square-pyramidal/trigonal-bipyramidal geometry around the central Fe(II) ion.

Table 2. Selected Bond Lengths (Å) and Angles (deg) of **1a** and **1b**

	[FeCl(depe)$_2$]BPh$_4$ (**1a**)	[FeBr(depe)$_2$]BPh$_4$ (**1b**)
Fe−P(1)	2.3340 (8)	2.3091 (7)
Fe−P(2)	2.2791 (9)	2.2800 (7)
Fe−P(3)	2.2740 (9)	2.2831 (7)
Fe−P(4)	2.3198 (9)	2.3184 (7)
Fe−X	2.3633 (9)	2.4892 (5)
	[FeCl(depe)$_2$]BPh$_4$ (**1a**)	[FeBr(depe)$_2$]BPh$_4$ (**1b**)
P(1)−Fe−P(2)	84.35 (3)	83.76 (3)
P(1)−Fe−P(3)	95.40 (3)	96.59 (3)
P(1)−Fe−P(4)	152.52 (4)	157.06 (3)
P(2)−Fe−P(3)	178.51 (4)	178.77 (3)
P(2)−Fe−P(4)	95.80 (3)	95.52 (3)
P(3)−Fe−P(4)	84.45 (3)	83.70 (3)
P(1)−Fe−X	106.37 (3)	101.62 (2)
P(2)−Fe−X	88.44 (3)	91.68 (2)
P(3)−Fe−X	90.22 (3)	89.41 (2)
P(4)−Fe−X	101.11 (3)	101.32 (2)

the following structural differences: the Fe−P bond lengths in **2a** range between 2.28 and 2.298 Å whereas the "axial" Fe−P bonds in **1a** are somewhat shortened (Fe−P(2) 2.279 Å, Fe−P(3) 2.274 Å) and the "equatorial" Fe−P bonds are significantly elongated (Fe−P(1) 2.334 Å, Fe−P(4) 2.320 Å). In addition, the Fe−Cl distance is larger by 0.052 Å in **1a** than in **2a**. Upon removal of N_2 from **2a** leading to **1a**, two of the Cl−Fe−P angles remain constant within ±2° while the other two are enlarged to 101° and 106°, respectively (vide supra). Similar results have been recorded for the analogous five-coordinate bromo system **1b** and its structural relationship with the corresponding octahedral bromo-N_2 complex **2b**.

Mössbauer Spectroscopy and Magnetic Susceptibility

Using Mössbauer spectroscopy, we showed earlier that the octahedral dinitrogen complex [FeCl(N_2)(depe)$_2$]BPh$_4$ (**2a**) loses dinitrogen at room temperature and that this process is reversible to some extent.[4] A second doublet in the Mössbauer spectrum of **2a** exhibiting a large quadrupole splitting of 2.64 mm/s (100 K) was assigned to the dinitrogen-free complex (δ_{IS} = 0.43(2) mm/s). In fact, the Mössbauer parameters of the five-coordinate complex **1a** prepared independently (δ_{IS} = 0.440(5) mm/s; ΔE_Q = 2.735(9) mm/s at T = 100 K) are almost identical to those of the presumably dinitrogen-free species in the matrix of **2a** and thus confirm our earlier assignment. Likewise, a second doublet was found in the Mössbauer spectrum of dinitrogen complex [FeBr(N_2)(depe)$_2$]BPh$_4$, **2b**, with parameters (δ_{IS} = 0.39(1) mm/s and ΔE_Q = 2.70 mm/s at 150 K) similar to those of the five-

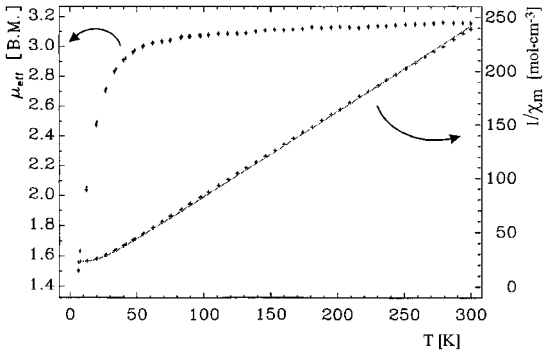

Figure 3. Effective magnetic moment μ_{eff} in μ_B (▼) and inverse molar susceptibility $1/\chi_m$ (+, diamagnetic contributions subtracted, along with a fit according to eq 1) of **1a** vs temperature (K).

coordinate bromo complex **1b** ($\delta_{IS} = 0.433(3)$ and $\Delta E_Q = 2.710(5)$ mm/s at 150 K).

To further characterize the five-coordinate species **1a** and **1b**, magnetic susceptibility data were recorded. Figure 3 shows the inverse molar susceptibility as well as the effective magnetic moment μ_{eff} of **1a** as a function of temperature. With a μ_{eff} of 3.1 μ_B at room temperature that is only slightly above the spin-only value for a triplet, the ground-state spin of **1a** must be $S = 1$ representing the "intermediate" spin state for Fe(II). Below 50 K, the magnetic moment sharply decreases ($\mu_{eff} = 1.5\ \mu_B$ at T = 7 K). Likewise, the inverse molar susceptibility follows Curie−Weiss law and becomes temperature-independent below 20 K. A similar behavior is observed for **1b**. From Mössbauer spectroscopy, antiferromagnetic ordering of the triplet molecules at low temperatures can be excluded. Rather, zero-field splitting of the $S = 1$ ground state with the $M_S = 0$ state lying at lowest energy is found to be the origin for the deviation from Curie's law. Consequently, the magnetic data of **1a** and **1b** are fitted with the spin-Hamiltonian[16,17]

$$\mathscr{H} = \mathbf{SDS} + \beta\mathbf{HgS} \qquad (1)$$

(**S** = spin-operator, β = Bohr magneton, **g** = g-tensor, **H** = magnetic field, **D** = zero-field splitting tensor). This leads to zero-field splitting parameter D of +35.6 (+30.7) cm^{-1} and g-values of $g_{||} = 2.516$ (2.223) and $g_{\perp} = 2.093$ (2.114) for **1a** (**1b**).

Thus, the X-ray, Mössbauer, and magnetic susceptibility results indicate a five-coordinate structure for **1a** and **1b** exhibiting an $S = 1$ ground state with a large zero-field splitting. The following section describes the full characterization of this ground state based on optical absorption spectroscopy coupled to an angular overlap model (AOM) analysis.

Optical Absorption Spectroscopy and AOM Parametrization

The electronic structure of compounds **1a** and **1b** was determined on the basis of AOM calculations on a [FeX(P)$_4$] (X = Cl, Br) model system of C_{2v} symmetry (Figure 4a). As the absorption spectra of **1a** and **1b** alone do not provide sufficient information to obtain the AOM e_σ and e_π ligand-field parameters of X and P,[18] **1a** and **1b** were treated simultaneously with the corresponding octahedral complexes [FeCl$_2$(depe)$_2$] (**3a**), [FeBr$_2$(depe)$_2$] (**3b**), and [FeHCl(depe)$_2$] (**4**) using one common set of parameters (Table 3). Restrictions to the parameter space were further imposed by the experimentally observed spin of the ground states, that is, $S = 0$ for the six- and $S = 1$ for the five-coordinate complexes, respectively.

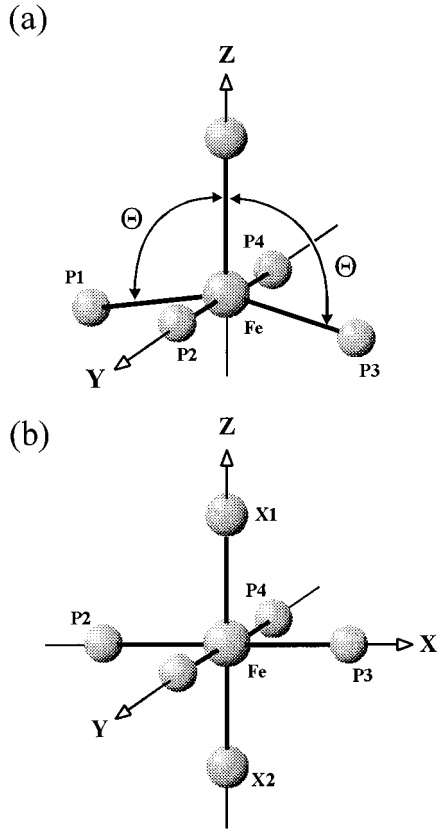

Figure 4. Structures of the model systems used for AOM calculations along with coordinate systems. (a) Model system [FeX(P)$_4$] for the compounds **1a** (X = Cl, Θ = 104°) and **1b** (X = Br, Θ = 101°). (b) Model system [Fe(X1)(X2)(P)$_4$] for the compounds **3a** (X1 = X2 = Cl), **3b** (X1 = X2 = Br), and **4** (X1 = H, X2 = Cl).

Table 3. AOM Parameters ($B = 650$, $C = 4B$, All Parameters in cm^{-1})

	Cl	Br	P	H
e_σ	4000	3300	7200	12000
e_π	1400	1800	300	0

The spectra of **3a**, **3b**, and **4** were fitted on the basis of model systems of D_{4h} (**3a**, **3b**) and C_{4v} symmetry (**4**), respectively (Figure 4b), and the results are listed in Table 4. The UV−vis spectra of dichloro and dibromo complexes **3a** and **3b** are closely related (Figure 5). Absorption bands at 14100 cm^{-1} (709 nm; $\epsilon = 70$ M^{-1} cm^{-1}) (**3a**) and 13320 cm^{-1} (751 nm; $\epsilon = 60$ M^{-1} cm^{-1}) (**3b**) can be assigned to transitions from the $^1A_{1g}$ ground state to the $^1E_g{}^a$ sublevel of $^1T_{1g}$ split in D_{4h}. The low-intensity transitions at 563 and

(16) Kahn, O. *Molecular Magnetism*, VCH Publishers: New York, 1993.
(17) Boyd, P. D.; Buckingham, D. A.; McMeeking, R. F.; Mitra, S. *Inorg. Chem.* **1979**, *18*, 3585−3591.
(18) (a) Larsen, E.; La Mar, G. N. *J. Chem. Educ.* **1974**, *51*, 633−640. (b) Schönherr, T. *Top. Curr. Chem.* **1998**, *191*, 88−111.

Table 4. Calculated and Observed Ligand Field Energies (kK) of Complexes **3a**, **3b**, and **4**

complex	method	$^1E_g{}^a$ $z^2 \leftarrow xz,yz$	$^1A_{2g}$ $x^2-y^2 \leftarrow xy$	$^1E_g{}^b$ $x^2-y^2 \leftarrow xz,yz$	$^1B_{2g}$ $z^2 \leftarrow xy$
[FeCl$_2$(depe)$_2$]	exptl[a]	14.1		24.6	
(**3a**)	AOM[b]	11.3	18.8	23.4	20.5
[FeBr$_2$(depe)$_2$]	exptl[a]	13.3		24.3	
(**3b**)	AOM[b]	9.3	18.8	22.2	18.8

		$^1E^a$	$^1A_2$	$^1E^b$	$^1B_2$
[FeHCl(depe)$_2$]	exptl[a]	21.5		26.0	
(**4**)	AOM[b]	19.1	18.7	27.0	28.6

[a] Measured in dichloromethane at room temperature. [b] Applying the parameters listed in Table 1.

609 nm, respectively, are attributed to an oxidized species forming via a five-coordinate intermediate because these transitions also appear in the spectra of **1a** and **1b** (see later). Obviously, the $^1A_{2g} \leftarrow {}^1A_{1g}$ transition is missing in the spectra of **3a** and **3b**, in agreement with the ligand field spectrum of the d^6 low-spin system [W(N$_2$)$_2$(depe)$_2$] which also has effective D_{4h} symmetry.[3b] In analogy, the absorption bands at 24630 cm^{-1} (406 nm; $\epsilon = 200$ M^{-1} cm^{-1}) (**3a**) and 24330 cm^{-1} (411 nm; $\epsilon = 220$ M^{-1} cm^{-1}) (**3b**) are assigned to the ^1E_g component of $^1T_{2g}$, $^1E_g{}^b$. The shift of the $^1E_g{}^a$ transitions to lower energy by ~40 nm in the spectrum of **3b** as compared to **3a** is caused by the smaller σ and higher π donating effect of the bromo compared to the chloro ligand (see also AOM parameters listed in Table 3); a much smaller shift to lower energy is observed for the $^1E_g{}^b \leftarrow {}^1A_{1g}$ band.

The spectrum of **4** exhibits an intense band at 21500 cm^{-1} (466 nm; $\epsilon = 950$ M^{-1} cm^{-1}) which is assigned to the transition $^1E_g{}^a \leftarrow {}^1A_{1g}$. This transition is significantly shifted to higher energy with respect to **3a** and **3b** because the hydrido ligand has a high σ-donor strength and lacks π-donor capacity. In addition, the intensity of this band is now much higher because the center of inversion is lost in the C_{4v} symmetry of this molecule, and thus, z^2-p_z mixing becomes effective. The corresponding $^1E^b \leftarrow {}^1A_1$ transition is calculated to be at 27000 cm^{-1} and may be related to the shoulder appearing in the spectrum at 26000 cm^{-1}. The intensity of this band is lower than that of the $^1E^a \leftarrow {}^1A_1$ transition, in contrast to the bis-halide systems **3a** and **3b** which have more intense $^1E_g{}^b \leftarrow {}^1A_{1g}$ transitions.

Optical absorption spectra of **1a** and **1b** are displayed in Figure 6. The absorption bands at 17790 cm^{-1} (562 nm) (**1a**) and 16470 cm^{-1} (607 nm) (**1b**) are caused by the reaction with O$_2$ because the intensity of these absorption bands increases when the solution is exposed to air. Removal of one halogen ligand in **3a** and **3b** or the hydrido ligand in **4** generates the d-orbital level scheme of **1a** and **1b**, respectively, which is given in Figure 7. Importantly, the z^2 orbital is significantly lowered in energy and now becomes populated, leading to an $S = 1$ ground state. On the other hand, the π donor action of the remaining halide ligand in conjunction with the bending of two phosphine ligands in the *xz* plane (cf. Figure 4a) puts the *xz* orbital at highest energy within the former t_{2g} orbital manifold. Shifting one electron from this orbital to z^2 leads to a $^3B_1$ [$(xz)^1(z^2)^1$] state

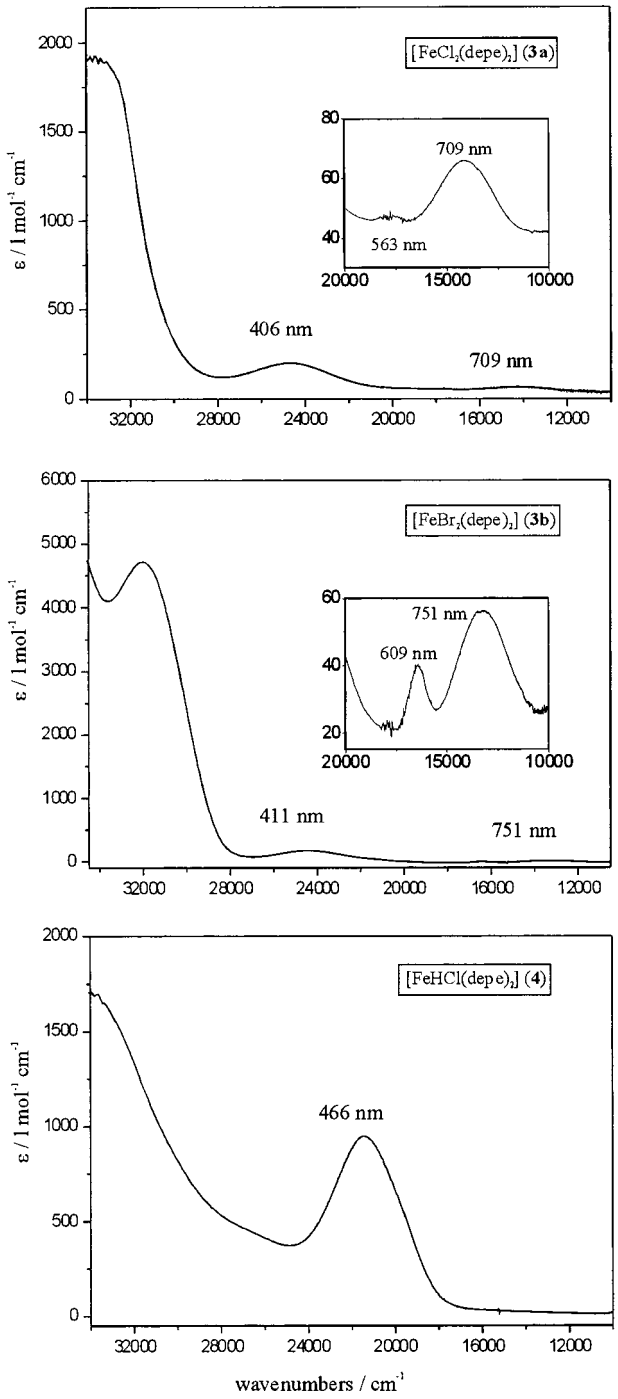

Figure 5. Optical absorption spectra of the octahedral complexes [FeCl$_2$(depe)$_2$] (**3a**), [FeBr$_2$(depe)$_2$] (**3b**), and [FeHCl(depe)$_2$] (**4**) in dichloromethane at room temperature.

which represents the triplet of lowest energy within the level scheme of Figure 7 and therefore the ground state of **1a** and **1b**.

Using the AOM parameters of Table 3, the lowest-energy ligand-field transitions of **1a** and **1b** ($^3A_2 \leftarrow {}^3B_1$; orbital transition $xz \rightarrow z^2$) are predicted to be at 8000 cm^{-1} (**1a**) and 7300 cm^{-1} (**1b**), respectively. Optical absorption spectra obtained on solid mulls show this band at 7500 cm^{-1} (1333 nm) (**1a**) and 7120 cm^{-1} (1404 nm) (**1b**), respectively (Figure 8). The other spin- and electric-dipole-allowed ligand field transitions corresponding to the d-orbital scheme of Figure

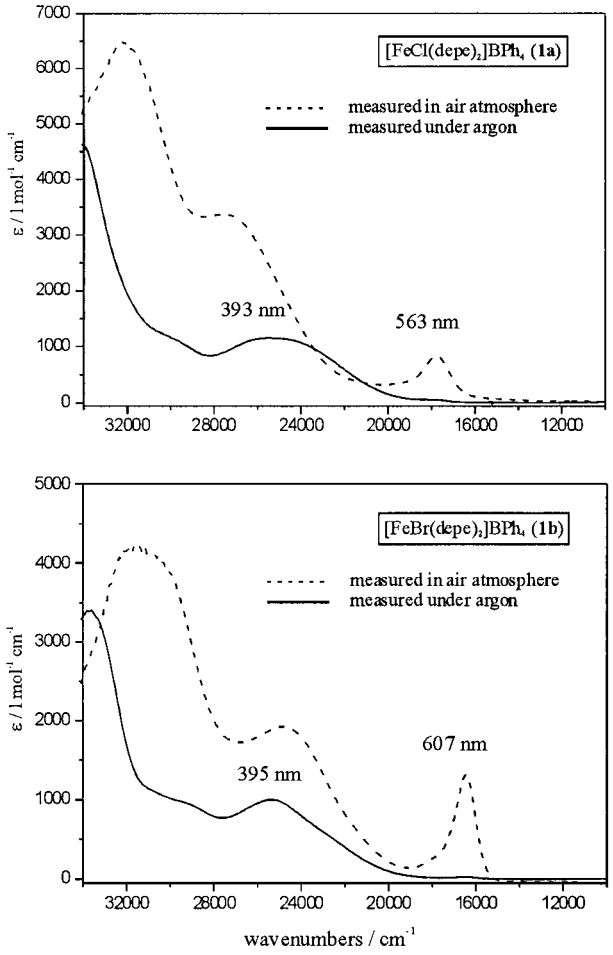

Figure 6. Optical absorption spectra of compounds **1a** and **1b** in dichloromethane at room temperature.

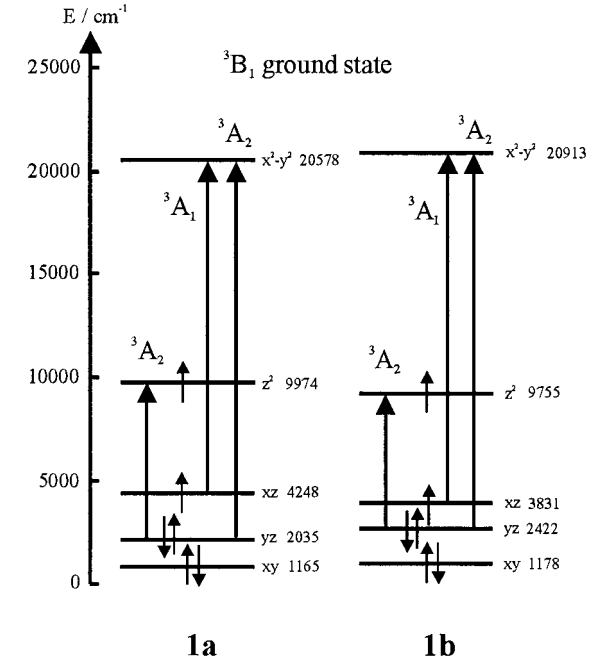

Figure 7. d-Orbital level scheme of compounds **1a** and **1b** obtained from the parameters of Table 3.

7 are listed in Table 5. However, the corresponding absorption bands are masked by features of much higher intensity

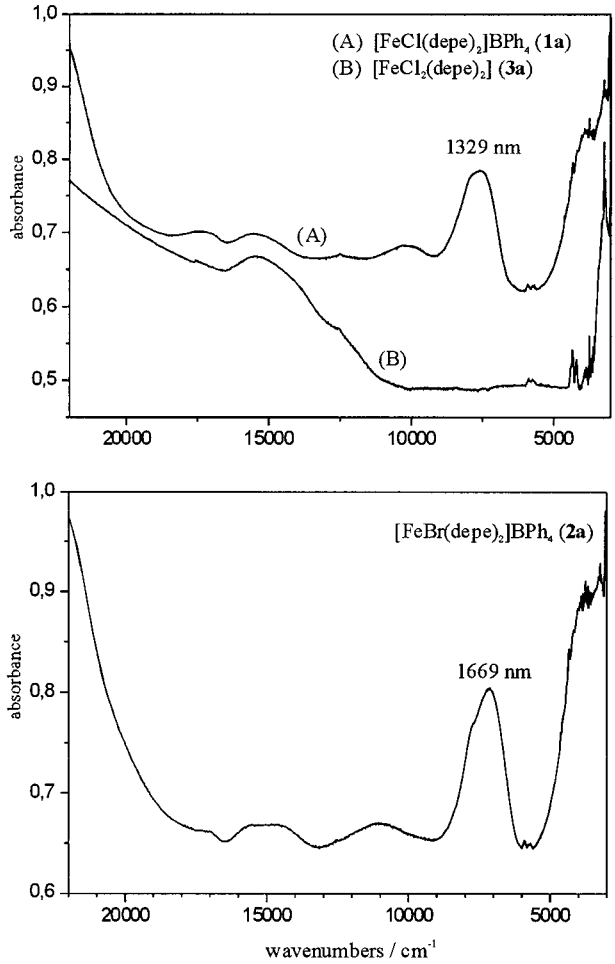

Figure 8. Optical absorption spectra of compounds **1a** and **1b** obtained on solid mulls between sapphire windows at 10 K.

Table 5. Calculated and Observed Transition Energies (kK) of Complexes **1a** and **1b**

complex	method	$^3A_2$ $z^2 \leftarrow yz$	$^3A_1$ $x^2-y^2 \leftarrow xz$	$^3A_2$ $x^2-y^2 \leftarrow yz$
$[FeCl(depe)_2]BPh_4$	exptl[a]	7.5[c]		
(**1a**)	AOM[b]	8.0	18.2	17.5, 18.3, 22.4[d]
$[FeBr(depe)_2]BPh_4$	exptl[a]	7.1[c]		
(**1b**)	AOM[b]	7.3	18.5	17.3, 18.1, 22.2[d]

[a] Measured in dichloromethane at room temperature. [b] Applying the parameters listed in Table 1. [c] Obtained on solid mulls between sapphire windows. [d] This orbital transition generates three $^3A_2$ states which split in energy because of spin coupling.

in the UV−vis region at 393 nm (**1a**; $\epsilon = 1150$ M^{-1} cm^{-1}) and 395 nm (**1b**; $\epsilon = 1000$ M^{-1} cm^{-1}) which correspond to CT transitions from halide and phosphine into empty or half-filled orbitals of the Fe(II) ion (Figure 6).

Discussion: Geometric/Electronic Structure of the Five-Coordinate Complexes and DFT Investigation of Their Spin-Forbidden Reaction with N_2

The spectroscopic and magnetic studies described in the preceding sections have lead to a definite assignment of the electronic ground state of five-coordinate systems $[FeX(depe)_2]BPh_4$, X = Cl, Br (**1a**,**1b**). While the magnetic susceptibility data indicated an $S = 1$ ground state exhibiting a zero-field splitting of 35 and 30 cm^{-1} for **1a** and **1b**,

respectively, optical absorption spectroscopy along with AOM calculations allowed us to fully characterize this electronic ground state as $^3B_1$ deriving from a $(xz)^1(z^2)^1$ configuration. In contrast, the corresponding six-coordinate dinitrogen complexes exhibit $^1A_{1g}$ ground states with $(t_{2g})^6$ configuration.[4] The shift of one electron from *xz* to z^2 in the five-coordinate fragment has been found to be due to three factors: (i) the energetic lowering of the z^2 orbital caused by removal of one axial ligand (N_2); (ii) the concomitant bending of two phosphine ligands away from the Fe−Cl bond raising the energy of the *xz* orbital through σ donation; and (iii) the further energy increase of this orbital by π-donation from the halide ligand. The combined effects of i−iii lead to a small separation between *xz* and z^2 (5700 cm^{-1}, Figure 7), thus favoring a triplet ground state.

The zero-field splitting calculated by the AOM was found to be very sensitive to the value of the P−Fe−P angle Θ (Figure 4). On the basis of a Θ value of 104° (average of 101° and 106° measured experimentally, cf. Figure 2) and a spin−orbit coupling constant ζ of 360 cm^{-1},[19] the $^3B_1$ ground state of **1a** was predicted to have a zero-field splitting of 200 cm^{-1}. The calculations showed the ground state to be further split by a rhombic splitting *E*, but this was found to be small (5 cm^{-1}). Increasing Θ to 106° lowers the zero-field splitting predicted for **1a** to 100 cm^{-1}. The difference to the experimentally determined value (36 cm^{-1} for **1a**, vide supra) is due to covalent mixing between metal d and ligand orbitals. On the basis of a Θ value of 101°, a zero-field splitting of 150 cm^{-1} is calculated for **1b**.

After the electronic and geometric structures of [FeX(N_2)(depe)$_2$]$^+$ and [FeX(depe)$_2$]$^+$, X = Cl (**2a**,**1a**) and Br (**2b**,**1b**), were established, it appeared of interest to investigate the energetics of N_2 binding in these systems by DFT calculations. As in earlier investigations, we chose the B3LYP functional combined with the LANL2DZ core potentials for the DFT calculations.[20] The geometry of the octahedral dinitrogen model complex [FeCl(N_2)($PH_2CH_2CH_2PH_2$)$_2$]$^+$ (**2a′**) shown in Figure 9, top, was obtained by optimizing the corresponding structure obtained from the crystal structure of **2a**,[4] simplified by replacement of the terminal ethyl groups of the depe ligands through hydrogen atoms. On the other hand, the ethylene bridges of these bidentate ligands were retained to obtain a realistic geometry. Five-coordinate model system [FeCl($PH_2CH_2CH_2PH_2$)$_2$]$^+$ (**1a′**) shown in Figure 9, bottom, was obtained by removing the N_2 ligand from the optimized structure of **2a′** and optimizing the resulting five-coordinate fragment. Selected bond lengths and angles for both optimized structures shown in Figure 9 are given in Table 6.

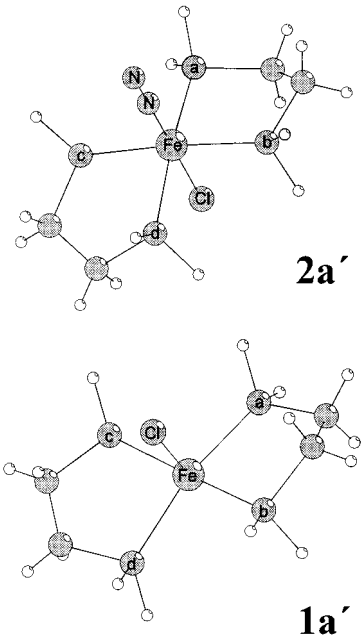

Figure 9. Optimized structures for model complexes **2a′** (top) and **1a′** (bottom).

Table 6. Selected Bond Lengths (Å) and Angles (deg) for the Optimized Structures of **2a′** and **1a′**

	[FeCl(N_2)-($PH_2CH_2CH_2PH_2$)$_2$]$^+$ (**2a′**)	[FeCl-($PH_2CH_2CH_2PH_2$)$_2$]$^+$ (**1a′**)
Fe−P(a)[a]	2.360	2.472
Fe−P(b)	2.366	2.367
Fe−P(c)	2.367	2.367
Fe−P(d)	2.360	2.472
Fe−Cl	2.365	2.370
P(a)−Fe−P(b)	84.76	83.36
P(b)−Fe−P(d)	94.49	97.80
P(c)−Fe−P(d)	84.76	83.36
P(b)−Fe−P(c)	171.49	173.90
P(a)−Fe−P(d)	169.39	158.27
P(a)−Fe−P(c)	94.49	97.80
P(a)−Fe−Cl	84.69	100.87
P(b)−Fe−Cl	85.97	86.95
P(c)−Fe−Cl	85.97	86.95
P(d)−Fe−Cl	84.69	100.87
Fe−N	1.850	
N−N	1.142	
N−Fe−Cl	180	

[a] The phosphine designations refer to Figure 9.

Fe−N and Fe−P distances in the octahedral, optimized structure **2a′** are slightly larger (about 0.07 Å) than experimental values, and the Fe−Cl distance is about 0.05 Å larger than that determined experimentally. The bite angle of the bidentate phosphine ligands is well reproduced (84.76° calcd vs 84.63° obsd). The decrease of the P−Fe−Cl angles from 90° observed experimentally, that is, the slight bending of the four phosphine groups toward the axial Cl ligand, is by 3°−4° higher than that observed. For five-coordinate fragment **1a′**, the calculation reproduces the bending of two phosphines away from Fe−Cl (P(a)−Fe−P(d) = 158.27°

(19) (a) Sugano, S.; Tanabe, Y.; Kamimura, H. *Multiplets of Transition Metal Ions*; Academic Press: New York, 1970. (b) Griffith, J. S. *The Theory of Transition-Metal Ions*; Cambridge University Press: New York, 1971.

(20) Frisch, M. J.; Trucks, G. W.; Schlegel, H. B.; Scuseria, G. E.; Robb, M. A.; Cheeseman, J. R.; Zakrzewski, V. G.; Montgomery, J. A., Jr.; Stratmann, R. E.; Burant, J. C.; Dapprich, S.; Millam, J. M.; Daniels, A. D.; Kudin, K. N.; Strain, M. C.; Farkas, O.; Tomasi, J.; Barone, V.; Cossi, M.; Cammi, R.; Mennucci, B.; Pomelli, C.; Adamo, C.; Clifford, S.; Ochterski, J.; Petersson, G. A.; Ayala, P. Y.; Cui, Q.; Morokuma, K.; Malick, D. K.; Rabuck, A. D.; Raghavachari, K.; Foresman, J. B.; Cioslowski, J.; Ortiz, J. V.; Stefanov, B. B.; Liu, G.; Liashenko, A.; Piskorz, P.; Komaromi, I.; Gomperts, R.; Martin, R. L.; Fox, D. J.; Keith, T.; Al-Laham, M. A.; Peng, C. Y.; Nanayakkara, A.; Gonzalez, C.; Challacombe, M.; Gill, P. M. W.; Johnson, B. G.; Chen, W.; Wong, M. W.; Andres, J. L.; Head-Gordon, M.; Replogle, E. S.; Pople, J. A. *Gaussian 98*; Gaussian, Inc.: Pittsburgh, PA, 1998.

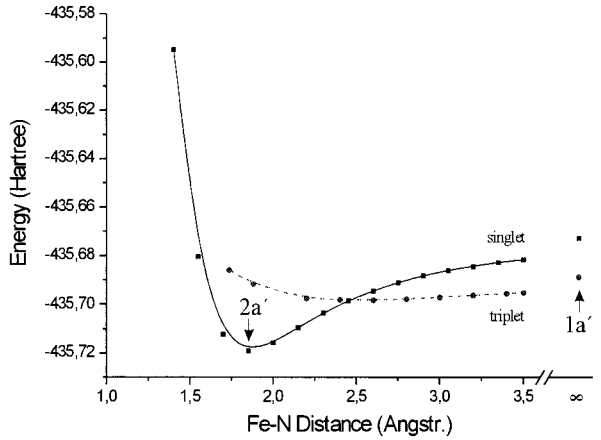

Figure 10. Relaxed potential energy surface (rPES) along the Fe−N coordinate for the reaction **2a′** ↔ **1a′** + N_2.

in **1a′** vs P(1)−Fe−P(4) = 152° in **1a**). However, the two other P-ligands are still slightly bent toward Fe−Cl in **1a′** (P(b)−Fe−Cl═P(c)−Fe−Cl = 86.95°) whereas these ligands are almost perpendicular to Fe−Cl in the real structure of **1a**. While the calculated Fe−P bond lengths are generally too large in **1a′** (by up to 0.15 Å), the calculation correctly reproduces the alternation of the Fe−P distances in this five-coordinate molecule; that is, the "bent" (or "equatorial") P-ligands have larger Fe−P distances than the "linear" (or "axial") ones (calcd, 2.472 vs 2.367 Å; expt, 2.32−2.33 vs 2.27−2.28 Å).

After determination of the optimized structures of the six-coordinate N_2 complex and the five-coordinate N_2-free fragment, a relaxed potential energy surface scan (rPES) along the Fe−N coordinate was generated. This means that for each point of the surface all structural parameters were optimized apart from the value of the Fe−N distance which was scanned from 1.4 to 3.5 Å. Figure 10 gives the rPES for the singlet state and the lowest triplet state of the system $[FeCl(depe)_2]^+ + N_2$ obtained in this manner. The figure also contains the energies for the fully dissociated system at r(Fe−N) = ∞. The triplet energy at this point corresponds to the ground-state energy of **1a′** plus the energy of free N_2 obtained at the same level of calculation (B3LYP/LANL2DZ). In agreement with the spectroscopic/AOM results, the triplet state is calculated to be the ground state at this fully dissociated configuration, and the $^1A_1$ state represents an excited state. In contrast, the $^1A_1$ state is the ground state at the Fe−N equilibrium distance, and the triplet state is an excited state at this geometry. Consequently, the singlet and the triplet state have to cross at some intermediate distance, and the rPES shows this crossover to occur at r(Fe−N) = 2.45 Å ≡ r_C. The transition between the two states $|...xz\alpha z^2\alpha\rangle$ (triplet) and $|...xz\alpha xz\beta\rangle$ (singlet) is enabled by spin−orbit coupling $\zeta\ \Sigma_i l_i \cdot s_i$ through the matrix element $\langle z^2\alpha|l_y \cdot s_y|xz\beta\rangle = -i3^{1/2} \cdot i/2$. As a consequence, the two surfaces repel each other in the manner of an avoided crossing (not shown in the figure), and the resulting lower hypersurface (corresponding to $E = E$(singlet) for $r < r_C$ and $E = E$(triplet) for $r > r_C$) defines the surface for bonding/dissociation of the N_2 ligand in the system $[FeCl(N_2)(depe)_2]^+ + N_2$. Qualitatively similar results are obtained from a nonrelaxed PES for a $[FeCl(PH_3)_4]^+ + N_2$ model system based on the equilibrium geometry of **1a**.[21] In contrast to this simpler treatment, however, the triplet potential surface in the rPES of Figure 10 appears almost flat between 2.0 and 3.5 Å with an extremely shallow minima around 2.8 Å. The almost dissociative character of the triplet surface provides an explanation for the marked photochemical lability of **2a** and **2b**.[22]

The spin-crossover along the Fe−N coordinate also affects the thermodynamic stability of Fe−N_2 complex **2a** with respect to loss of N_2. Retaining a singlet state s, the reaction enthalpy for release of N_2 from $[FeCl(N_2)(depe)_2]^+$ would be $\Delta E°_s = \Delta H°_s = 28.21$ kcal/mol (zero-point vibrational energy corrected by $^1/_2 hc\tilde{\nu} = 0.7190$ kcal/mol for $\tilde{\nu}$ (Fe−N) = 503 cm^{-1} [10a]). However, the crossing of the triplet state t becoming ground state of the system for Fe−N distances larger than r_C = 2.45 Å lowers the reaction enthalpy for release of N_2 by E_s(Fe−N = ∞) − E_t(Fe−N = ∞) = 10.09 kcal/mol, resulting in an effective $\Delta E°$ value for N_2 release of 18.27 kcal/mol. These values have been calculated for the gas phase, but on the basis of the conservation of charge during the reaction, no major contributions of the solvation energy are expected in condensed phase. Because of the liberation of N_2, the entropy change $S°$ for this reaction at 300 K is estimated to approximately correspond to the entropy of free N_2 at 300 K, $S(N_2; 300\ K) = 192$ J/mol·K,[23] corrected for the loss of entropy stored in the Fe−N_2 bond (about 3 J/mol·K for $\tilde{\nu}$ (Fe−N) = 503 cm^{-1} [23]); the contributions to the entropy due to all other modes are neglected. This leads to an effective entropy change of 189 J/mol·K for release of N_2, so that a free reaction enthalpy $\Delta G° = \Delta H° - T\Delta S°$ of 4.7 kcal/mol for N_2 release (or −4.7 kcal/mol for N_2 bonding) results at 300 K. This value is in agreement with a thermally allowed reaction confirming the observed thermal instability of $[FeCl(N_2)(depe)_2]$ regarding the loss of N_2.

Analogous PES calculations on N_2 dissociation from the hydride-containing model complex $[FeH(PH_3)_4(N_2)]^+$ indicate that for all Fe−N distances the singlet state is ground state and no spin-crossover along the Fe−N coordinate occurs.[21] In the hydrido complexes, the z^2 orbital is raised by a very strong σ-antibonding interaction so much in energy that its involvement in a triplet ground state becomes impossible. Moreover, the energy of the *xz* and *yz* orbitals involved in the back-bonding of N_2 is *not* increased by π donation from the *trans* ligand which in the case of the halogeno systems **2a** and **2b** has been found to be one of the factors that contribute to the lability of the Fe−N_2 bond. Therefore, *trans* hydrido N_2 systems should have an intrinsically higher termodynamic stability than their *trans* halide counterparts, in agreement with the observation. More

(21) Lehnert, N. PhD. dissertation, University of Mainz, 1999.
(22) There exists considerable difficulty to converge the triplet state around 2 Å, probably because of orbital level crossing within the lowest triplet states at about this distance.
(23) Moore, W. J.; Hummel, D. O. *Physikalische Chemie (Physical Chemistry)*; Walter de Gruyter: Berlin, 1976.

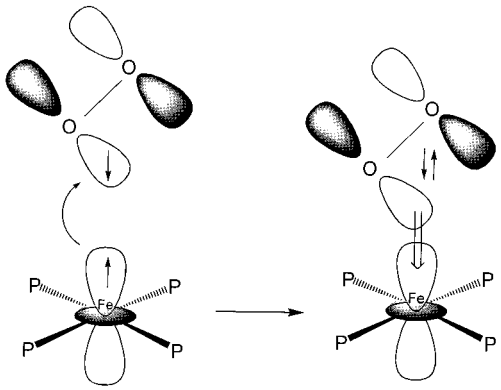

Figure 11. Reaction of **1a′** and **1b′** with dioxygen (schematically).

detailed investigations on the electronic structure of Fe(II) hydrido−N_2 complexes will be presented in a forthcoming paper.[12]

Electronic−structural differences may also explain the observed reactivity differences toward dioxygen between analogous hydrido and halogeno phosphine complexes: the five-coordinate halogeno systems having an unpaired electron in the z^2 orbital react with O_2 in the usual manner by transferring this electron into the O_2 π^* orbital and binding to O_2^- as Fe(III) (Figure 11). Therefore, solutions of these ions are extremely air sensitive. In contrast, the z^2 orbital is unoccupied in the corresponding hydrido systems (vide supra), making this reaction path with O_2 impossible. This explains the stability with respect to O_2 of $[FeH(dppe)_2]^+$ fixing dinitrogen from air.[10b] Thus, the complementary reactivity between otherwise related hydrido and halogeno phosphine complexes with respect to N_2 and O_2 (hydrido, inertness toward O_2, favorable reaction with N_2; halogeno, favorable reaction with O_2, low affinity toward N_2) can be traced back to the characteristic differences in their electronic structure.

Acknowledgment. F.T. thanks P. Gütlich (University of Mainz) for measuring time on his Mössbauer and magnetic susceptibility setups as well as W. Tremel (University of Mainz) and W. Bensch (University of Kiel) for measuring time on their X-ray diffractometers. Funding of this research by Deutsche Forschungsgemeinschaft (DFG Tu58/07) and Fonds der Chemischen Industrie (FCI) is gratefully acknowledged.

Supporting Information Available: Lists with atomic coordinates and isotropic and anisotropic displacement parameters as well as bond lengths and angles for **1a** and **1b**. Crystallographic information in CIF format. This material is available free of charge via the Internet at http://pubs.acs.org.

IC0111987